sciendo

Ekológia (Bratislava) - Journal of the Institute of Landscape Ecology, Slovak Academy of Sciences Vol. 44, No. 2, p. 212–222, 2025
DOI:10.2478/eko-2025-0024

REMOTE SENSING OF SURFACE TEMPERATURE AND LAND USE CHANGES IN SEMI-ARID CLIMATE

MAYA BENOUMELDJADJ ✉[1], NEDJOUA BOUARROUDJ[2], ABDELOUAHAB BOUCHAREB[3], MALIKA RACHED-KANOUNI[4], NORHANE CHOUITER[5]

[1]Larbi Ben Mhidi University Oum El Bouaghi, Department of Architecture, Earth Sciences and Architecture Faculty, AUTES Research Laboratory, University of Constantine 3, Salah Boubnider, Constantine city, Algeria; e-mail: maya.benoumeldjadj@univ-oeb.dz
[2]Salah Boubnider University of Constantine 3, AEEE Research Laboratory University of Salah Boubnider, Constantine 3, Algeria; e-mail: nedjoua.bouarroudj@univ-constantine3.dz
[3]Salah Boubnider University of Constantine 3, AUTES Research Laboratory, University of Constantine 3, Algeria; e-mail: abdelouahab.bouchareb@univ-constantine3.dz
[4]Larbi Ben M'hidi Universityof Oum El Bouaghi, AUTES Research Laboratory, University of Constantine 3, Algeria; e-mail: malika.rached@univ-oeb.dz
[5]Laboratory of Functional Ecology and Environment, Department of Nature and Life Sciences, Faculty of Exact Sciences, Nature and Life Sciences, University of Larbi Ben M'hidi, Oum El Bouaghi, Algeria; e-mail: chouiter.norhane@univ-oeb.dz

✉ Corresponding author

Received: 24 April 2025 / **Accepted:** 12 August 2025

Abstract

Benoumeldjadj M., Bouarroudj N., Bouchareb A., Rached-Kanouni M., Chouiter N.: Remote sensing of surface temperature and land use changes in semi-arid climate. Ekológia (Bratislava), Vol. 44, No. 2, p. 212–222, 2025.

In the context of global climate change, cities can be affected by the phenomenon of urban heat island (UHI), which generates temperature differences between a city and the adjacent rural region. The impacts and challenges of UHI on urban systems are numerous and thus question the strategies to deal with them. The aim of this study is to identify the presence of UHI in the territory of Aïn M'lila (eastern Algeria), to understand their spatial distribution according to the changes in urban land use (land use/land cover [LULC]), and to suggest ways to reduce their effect. The method adopted, involving remote sensing using Landsat satellite images and the Google Earth Engine platform, enables an initial diagnosis to be made of the effect of UHI on this area by quantifying it and establishing its correlation with normalized difference vegetation index (NDVI) and land surface temperature (LST) over the period 2005–2023. The analyses of LULC, NDVI, and LST revealed a significant urban expansion, characterized by an increase in impermeable surfaces of 2%–7% and a reduction in cultivated land. This urbanization led to a significant rise in surface temperatures, with peaks reaching 49.37 °C in 2005. Despite a slight improvement in 2023, due to greening initiatives, the study highlights the persistence of UHI effects. The results highlight the need for urban project approaches and green urban planning to analyze and propose planting in sectors subject to UHI effects. However, there is a need for contextualized local climate policy integrating adaptation strategies to exploit the reversibility potential of urban spaces as best as possible.

Key words: Aïn M'lila, climate data, urban heat island, urban land use, surface temperature, NDVI.

Introduction

Urbanization results in the transformation of natural landscapes into impermeable surfaces, leading to a significant change in the albedo, thermal properties of surfaces, and humidity of urban areas. This results in cities being warmer than their surroundings. This phenomenon, known as the urban heat island (UHI) (Aleksandrowicz et al., 2017), has been the subject of air temperature measurements in many cities around the world for UHI diagnosis, such as Dijon (Richard et al., 2018), Lyon (Renard, Alonso, 2020), Florianópolis Nanjing (Da Rocha et al., 2019; Yang et al., 2020), and Sydney (Yun et al., 2020).

According to IPCC forecasts (IPCC, 2022), urban temperatures are set to rise because of climate change. This will lead to various issues affecting the future of urban environments, including the health and vulnerability of populations, increased energy consumption, and a deterioration in thermal comfort conditions (Santamouris, 2020; Nieuwenhuijsen, 2021).

Many studies have commented on the causes of the effects of UHI: increase in impermeable areas, disappearance of natural spaces, disruption of ventilation, disruption of radiative exchanges, and generation of anthropogenic heat (Imran et al., 2021).

Understanding UHI is, therefore, both an environmental and public health issue for which the development of mitigation measures requires in-depth investigation within the framework of a scientific approach. UHI intensity, a phenomenon first identified in 1818, refers to the increase in atmospheric temperatures (Ta) and land surface temperatures (LSTs) in urban areas com-

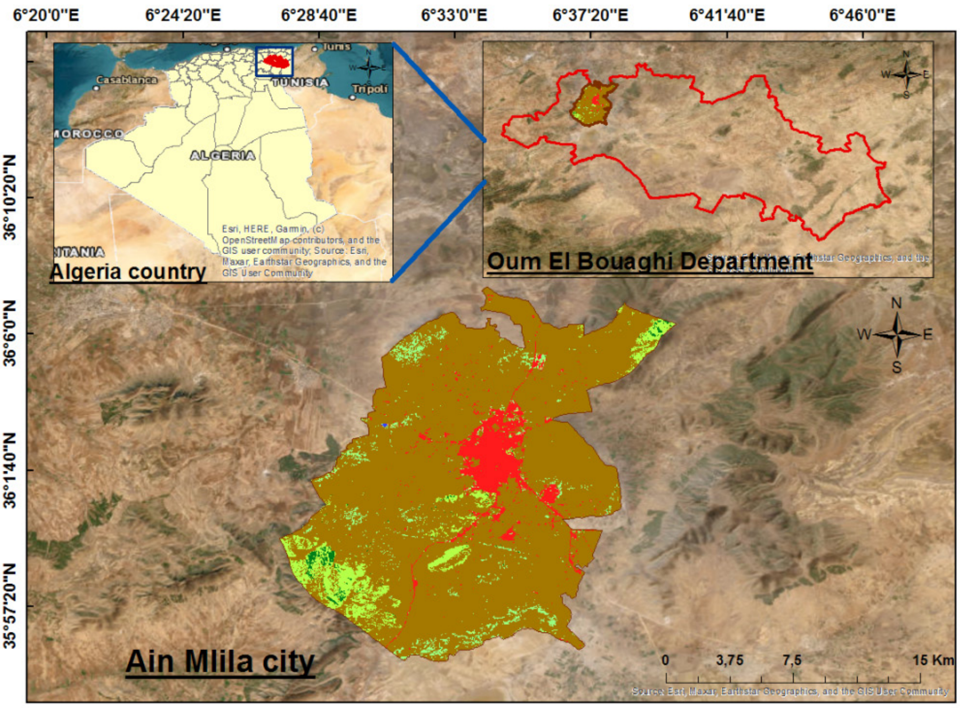

Fig. 1. Location map of Aïn M'lila (Algeria).

pared to surrounding rural areas (Estoque, Murayama, 2017), derived from measurements made by sensors on board satellites (Chan et al., 2021).

The study of LST provides information on the spatiotemporal variations and surface equilibrium state (Charfi, Dahech, 2018; Renard et al., 2019). LST is widely used in various studies, including climate change, vegetation cover monitoring, UHIs, and environmental studies (Hashemi et al., 2023). This temperature changes in space and time with changing climatic conditions and human activities (Anandababu et al., 2018). Global urbanization has significantly impacted the level of greenhouse gases in the atmosphere and reshaped landscapes. This urbanization has important climate implications on several scales, including UHIs, due to the simultaneous transformation of the natural land cover and the introduction of urban material. Surveys are long, cumbersome, and expensive, highlighting remote sensing as an obvious and preferred alternative to monitor these climate implications.

The size of the ICU effect may vary depending on the land-use/land-cover (LULC) model, city structure, city size, seasonal variations, environmental context, urban engineering, topography, and area location (Shojaei et al., 2017).

The overall objective of this research is to identify UHI for the city of Aïn M'lila (Algeria) in relation to LULC. To meet this overall objective, two secondary objectives were stated. The first aims to determine UHI on the territory of the city that will be prioritized for adaptations and interventions in the event of an alarming situation. The second objective is to calculate a standardized vegetation index (normalized difference vegetation index [NDVI]) in order to have an understanding of the plant architecture and to assess the link with LST and UHI.

Material and methods

Study area

The Aïn M'lila region, located in eastern Algeria between 36°02'00" North and 6°35'00" East, at an altitude of 771 m, is part of the external zones of the Alpine chain in eastern Algeria (Fig. 1). Situated in the southern high plains of the Constantine region, this area is bordered by Constantine to the north, Batna to the south, Oum-El-Bouaghi to the east, and Mila to the west. It covers approximately 23,602.5754 ha and has a population of about 88,441 inhabitants.

It has a continental climate characterized by significant seasonal temperature variations. Winter temperatures range from 0 to 12 °C, with glacial winds and occasional snowfall, while summer temperatures can soar between 25 and 40 °C, resulting in dry and hot conditions. Average annual precipitation is about 200–400 mm, with the majority occurring in winter, coinciding with maximum rainfall, while summer often experiences thunderstorms. Spring is marked by significant frosts and autumn brings milder temperatures, making the overall climate distinct and variable throughout the year.

Data source

This research focuses on the time series of the UHI effect in Aïn M'lila by analyzing land cover changes and vegetation loss over four periods: 1995, 2005, 2015, and 2023. Landsat 5 and 7 image data acquired for this period were utilized through the Google Earth Engine (GEE) platform (Gandhi, 2022; Benoumeldjadj et al., 2024).

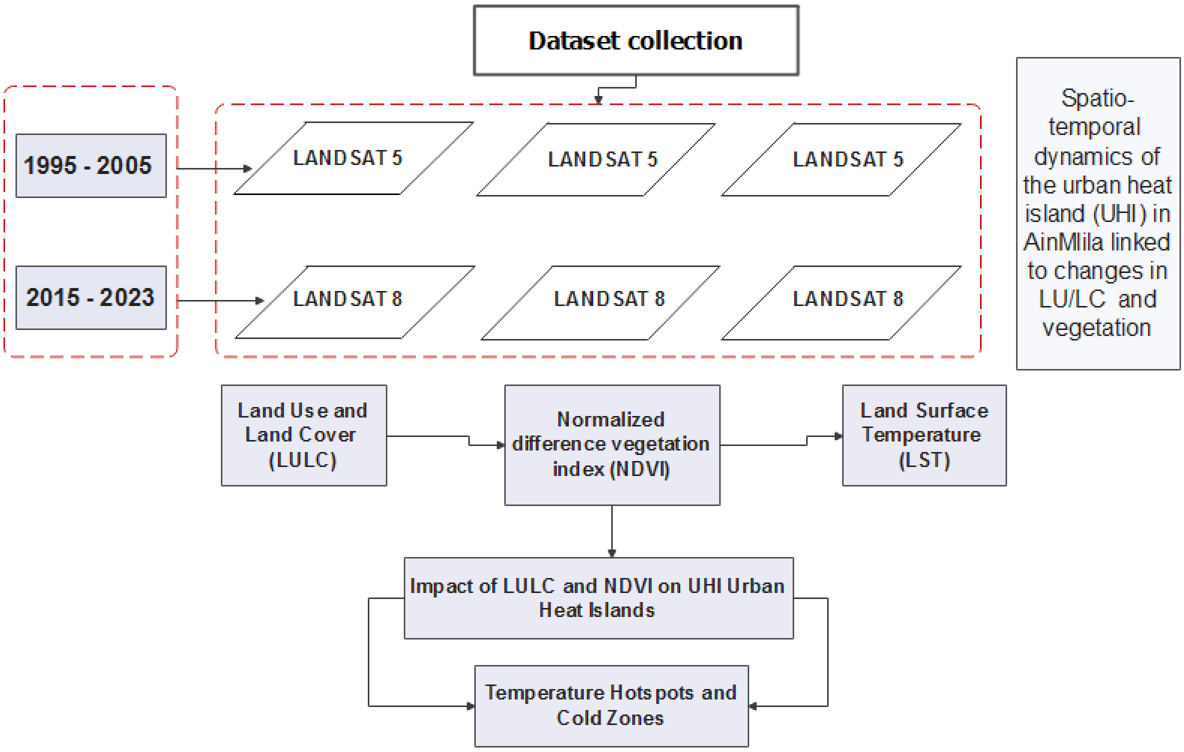

Fig. 2. Flowchart of the study.

Bands 1–5, as well as band 7 were used to classify LULC types using a supervised method, employing maximum likelihood classification. In addition, thermal band 6 was used to estimate LST values. Bands 1–5 and 7 have a spatial resolution of 30 m, while thermal band 6 has a resolution of 120 m for Landsat 5 and 60 m for Landsat 7, though resampled to 30 m. This examination requires locating fine changes in surface reflectance to understand the processes of change and their impact on temperature in the study areas (USGS.gov, 2019).

To complement the analysis, temporal variations in the data were also considered to better understand the evolution of LULC and its impact on surface temperatures. The integration of NDVI data allowed for the assessment of vegetation health in the study areas, providing valuable information on vegetation cover and its influence on local temperatures. In parallel, the analysis of LST values helped identify high-heat zones, often correlated with urban surfaces or deforested areas.

The analysis of the relationship between LULC changes and the intensity of LST, as well as the UHI effect during the 4-year study period requires Landsat images. The indicators calculated from the remote sensing data are NDVI and LST.

NDVI determination

This index uses the red (Red) band in the visible spectrum and the near-infrared (NIR) band. Indeed, chlorophyll absorbs energy in the visible 400–700 nm (red band) and reflects strongly in the infrared 800–900 nm. This is why, these two bands are particularly effective in describing vegetative activity on the surface of the globe. Thus, NDVI has proven to be a robust indicator for the analysis of spatiotemporal changes in vegetation growth and distribution (Ellili et al., 2019), vegetation stress (Beisel et al., 2018), and vegetation productivity (Zeng et al., 2020).

NDVI is a vegetation index particularly suited to monitoring the health of vegetation (Guo et al., 2018). High chlorophyll activity implies high biomass, and therefore high NDVI value. The NDVI formula is as follows:

$$\mathrm{NDVI} = (\mathrm{NIR} - \mathrm{Red})/(\mathrm{NIR} + \mathrm{Red}), \qquad (1)$$

where NIR and Red refer to specific light wavelengths captured by satellite sensors. NDVI values range from −1 to +1, with higher values (0.6–0.9) indicating healthy, dense vegetation, values around 0 showing little to no vegetation, and negative values often associated with water (sand, rock, snow, water) or where vegetation is senescent (Benoumeldjadj et al., 2023).

Estimation of the earth's surface temperature

Estimation of LST through thermal remote sensing only provides measurement of the surface radiant temperature primarily emitted by the ground. This quantity can be converted into brightness temperature, which is affected by various atmospheric effects and also by the fact that the earth's surface is not a perfect black body for thermal emission (Wang et al., 2015). Therefore, the pursuit of an accurate LST becomes more complicated as both soil and atmospheric effects must be considered.

LST represents the temperature of the top layer of the ground. It plays a crucial role in the distribution of energy between soil and vegetation and significantly influences air temperature.

LST can be obtained from thermal data provided by satellites. To convert Landsat thermal data into LST values, a two-step process is used:

(i) Conversion of thermal band DNs value into top-of-atmosphere radiance (Khamchiangta, Dhakal, 2019), calculated with the equation

$$L_\lambda = ((L_{max} - L_{min})/(Q_{CAL\ max} - Q_{CAL\ min})) \times (DN - Q_{CAL\ min}) + L_{min,} \quad (2)$$

where L_λ is the luminance of the upper atmosphere in watts (m^2 × sr × μm) and DN is the numerical value of the Landsat 6 thermal band. $Q_{CAL\ max}$ = 255 and $Q_{CAL\ min}$ = 0 for products processed before 4/5/2004 and 1 for products processed after 4/5/2004, L_{max} and L_{min} are in watts/(m^2 × sr × μm), and values are provided in the Landsat image data metadata file.

(ii) Estimation of LST (and atmospheric correction) by inversion of equation:

$$L_{sens,\lambda}=[\in_\lambda B_\lambda(T_s)+(1-\in_\lambda)L_\lambda\downarrow]\tau_\lambda+L_\lambda\uparrow, \quad (3)$$

where $L_{sens},_\lambda$ is the luminance at the sensor level at the top of the atmosphere, $\in_\lambda$ is the surface emissivity, and $B_{\lambda(Ts)}$ is the radiance emitted by a black body at temperature *Ts*, calculated using Planck's law. $L_\lambda\downarrow$ is the downward atmospheric luminance, τ_λ is the total atmospheric transmissivity, and $L_\lambda\uparrow$ is the upward atmospheric luminance.

LST is retrieved from (ii) by inverting Planck's law, known as surface emissivity. The main objective of this study is to analyze the evolution and characteristics of UHI in Aïn M'lila, in relation to changes in LULC over a period of 28 years (1995–2023). Figure 2 presents the methodological flowchart summarizing the main data processing steps and calculation of indicators.

The LULC classification was carried out in three distinct phases. First, using the shapefile of the municipality derived from the Feature Collection ("FAO/GAUL/2015/level2") (Gandhi, 2022), areas were selected based on points on representative pixels of the LULC classes. Next, a supervised maximum likelihood classification was applied to the Landsat images using scripts within GEE. Finally, an accuracy assessment was conducted on all the produced LULC maps, thereby ensuring the reliability of the classification results for landscape change analysis.

The methodology is based on the use of the zonal statistics tool in ArcMap. This tool allows to calculate and analyze the maximum and minimum values of LST within each district or defined zone (Chen, Zhang, 2017). This approach provides a clear visualization of the spatial distribution of temperatures, highlighting thermal contrasts at the scale of the studied territory.

The results of image classification to generate LULC maps, NDVI calculation, and LST estimation highlight the correlations between LST and LULC, quantify the intensity of UHI, and reveal urban expansion and warming trends over nearly three decades. This multidimensional approach aims to provide crucial insights for urban planning and local climate management in Aïn M'lila.

Results and discussion

LULC evolution

The use of satellite images reveals the dynamics of landscape transformation: distribution of agricultural areas, deforestation, and urban sprawl. In this context, the processing of geospatial data has been the subject of considerable and continuous attention since the launch of the first satellite missions (Pei et al., 2021; Fagan, Defries, 2024). Data from Landsat 5 and 8 images are used using the GEE platform to assess LULC changes in the study area (Aïn M'lila) for 1995, 2005, 2015, and 2023.

A supervised classification by maximum likelihood made it possible to distinguish seven land cover classes: cropland, forest, shrubland, grassland, impervious surfaces, bare areas, and water body/salt marsh. Validation by confusion matrix indicates excellent reliability of the mapping (Kappa index ranges from 0.79 in 1995 to 0.91 in 2023). The spatiotemporal distribution and patterns of LULC changes and persistence are presented in Fig. 3.

Throughout the study period, cropland was the dominant land use type. Its area decreased from 21,253.66 ha in 1995 to 19,936.12 ha in 2023 of the total area (23,602.57 ha) (Table 1). This indicates increasing pressure on arable land, potentially due to urbanization, as Aïn M'lila is an agriculture-oriented region. The proportion of forest remained relatively stable, maintaining around 142.78 ha during the study period, due to a lack of significant reforestation or substantial changes in forest cover.

Except for 2005, when shrubland initially experienced a slight decrease of 4%; in other years, this decrease remained stable at approximately 158 ha. This stability indicates resilience to urbanization or other pressures. The proportion of grassland has remained constant at 615.33 ha since 1995, after a slight increase to around 1,018.38 ha in 2005. This stability at 3% indicates resilience, and this fluctuation could reflect variations in climatic conditions or land management practices. Grasslands provide important habitats for many species and play a crucial role in water cycles, contributing to filtration and water resource management.

The proportion of impervious surfaces increased significantly from 487.76 to 1,542.67 ha between 1995 and 2015 (Figs 4 and 5). This trend toward urbanization is indicative of growing urban expansion and infrastructure development in the region (Attar, Saraoui, 2021). The stability of the proportion at 7% from 2015 to 2023 (Fig. 5) (1,534 ha) may indicate some control or slowdown of urbanization due to the precarious housing resorption program (RHP) and urban planning policies. The presence of impervious surfaces (built-up areas) is concerning, as it can lead to increased rainwater runoff, cause flooding, and degrade surrounding ecosystems (Yasser, 2021).

The proportion of bare areas remained extremely low during the period from 1995 to 2023, with a slight increase in 2005 followed by stabilization. It is essential to note that this low value also indicates a relative absence of significant land degradation, though it should not be overlooked. Regarding rivers and salt marshes, the year 2005 (Figs 4 and 5) was marked by their absence, with a low recorded area of 0.508 ha, signaling the beginning of the establishment of these ecosystems in the region. This upward trend continued, with a further increase in 2015 (0.603 ha) and significant growth reaching 3.93 ha in 2023 (Table 1).

Algeria has experienced an intense and persistent drought over the past 20 years. This drought, characterized by a significant rainfall deficit, has affected the whole of Algeria, particularly its northeastern part, of which the study area is a part. But the most severe and persistent are those of the last two decades, which were characterized by a rainfall deficit of around 13% for the eastern region. This drought has had a negative impact on the flow regime of the wadis, recharge of the water table, and the filling level of the watercourses (Achite et al., 2017).

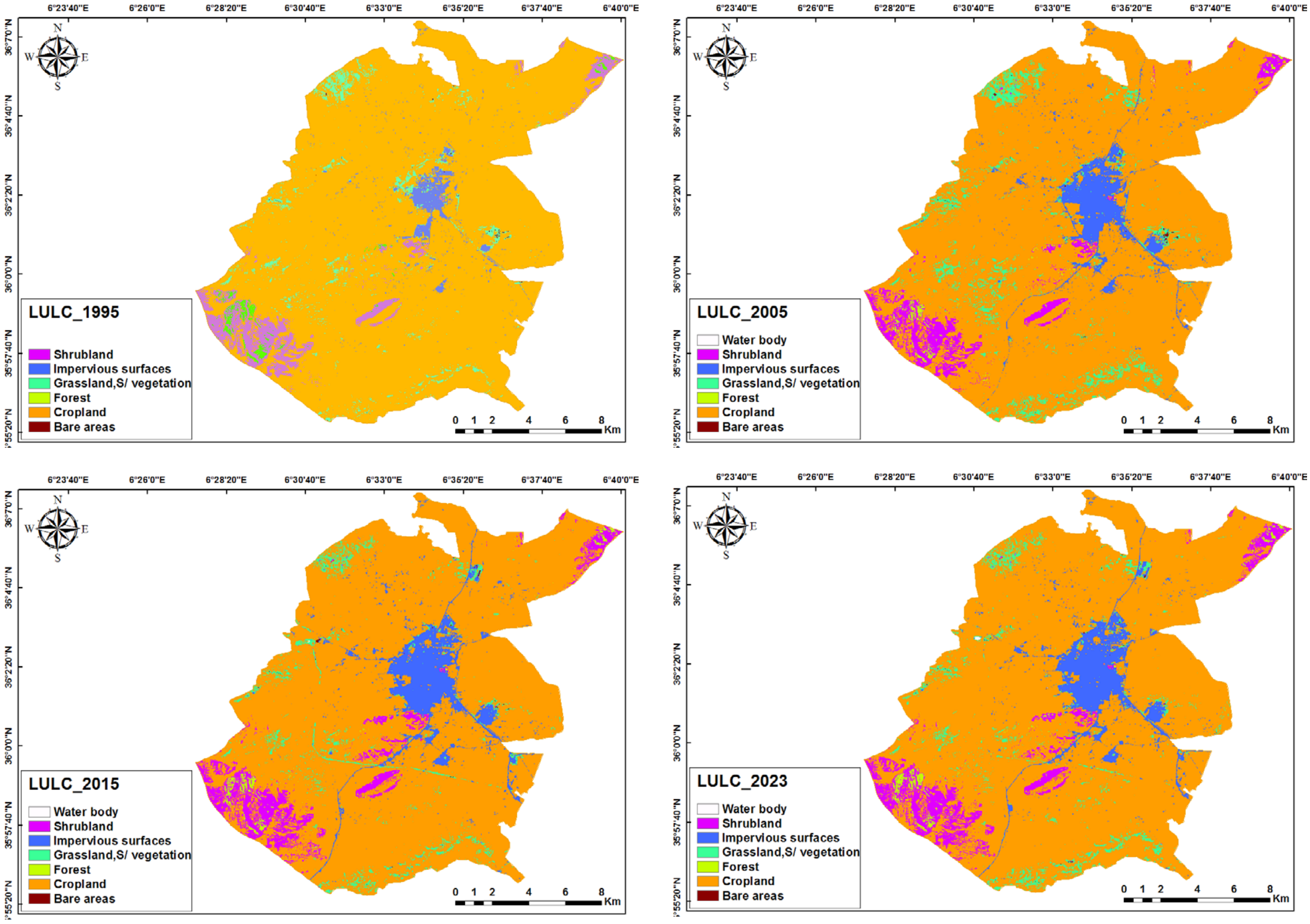

Fig. 3. Land use and land cover in Aïn M'lila from 1995 to 2023.

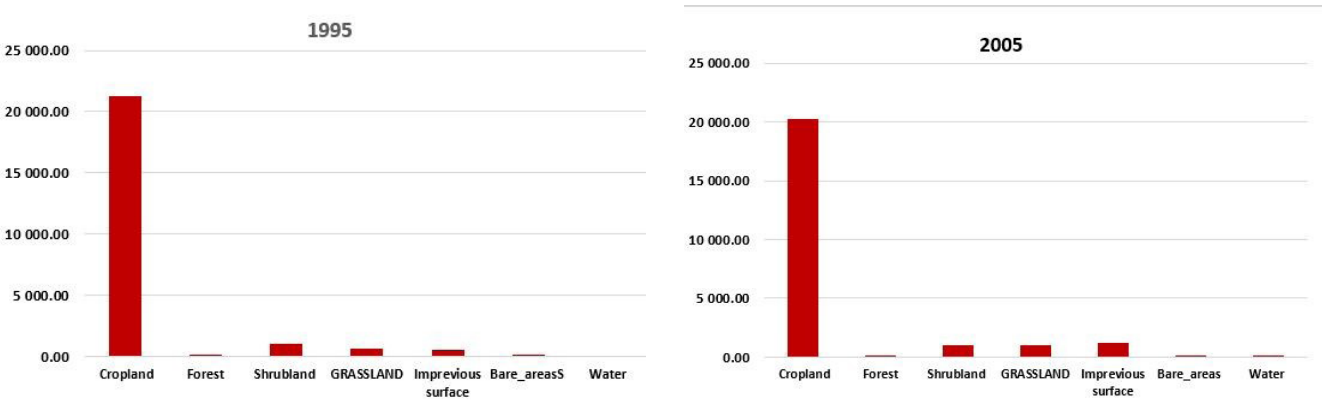

Fig. 4. LULC graph of 1995 and 2005.

Impact of land use changes on NDVI from 1995 to 2023

NDVI is a vegetation index used to determine land use. The values of this index give a matrix of values between −1 and 1, characterizing the NDVI of each pixel in the image. Values between −1 and 0 represent elements composed of water, values between 0 and 0.25 represent elements composed of soil, and values between 0.25 and 1 characterize vegetation.

The higher the index, the denser the vegetation. To associate an index with each pixel in an image, the indices were classified into three categories: low vegetation index (NDVI between 0.25 and 0.5), mid vegetation index (NDVI between 0.5 and 0.75),

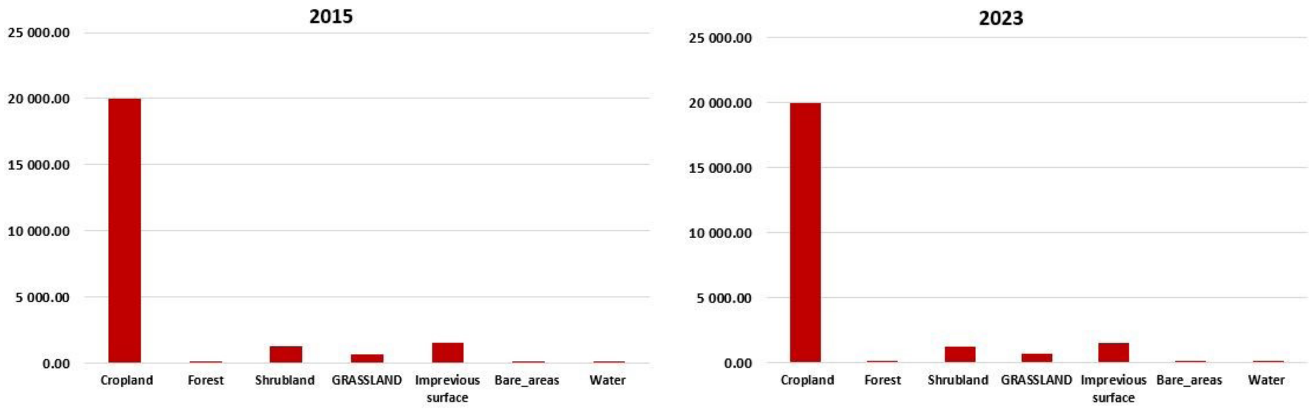

Fig. 5. LULC graph of 2013 and 2023.

Table 1. Land use and land cover types.

	Cropland (ha)	Forest (ha)	Shrubland (ha)	Grassland (ha)	Impervious surface (ha)	Bare areas (ha)	Water (ha)
1995	21,253.66	171.69	1,064.64	615.66	487.77	9.15	
2005	20,228. 31	106.18	1,008.58	1018.38	1,227.98	12.64	0.51
2015	20,009.34	142.79	1,238.73	658.44	1,542.68	9.95	0.65
2023	19,936.13	157.96	1,251.95	709.64	1,534.69	8.28	3.92

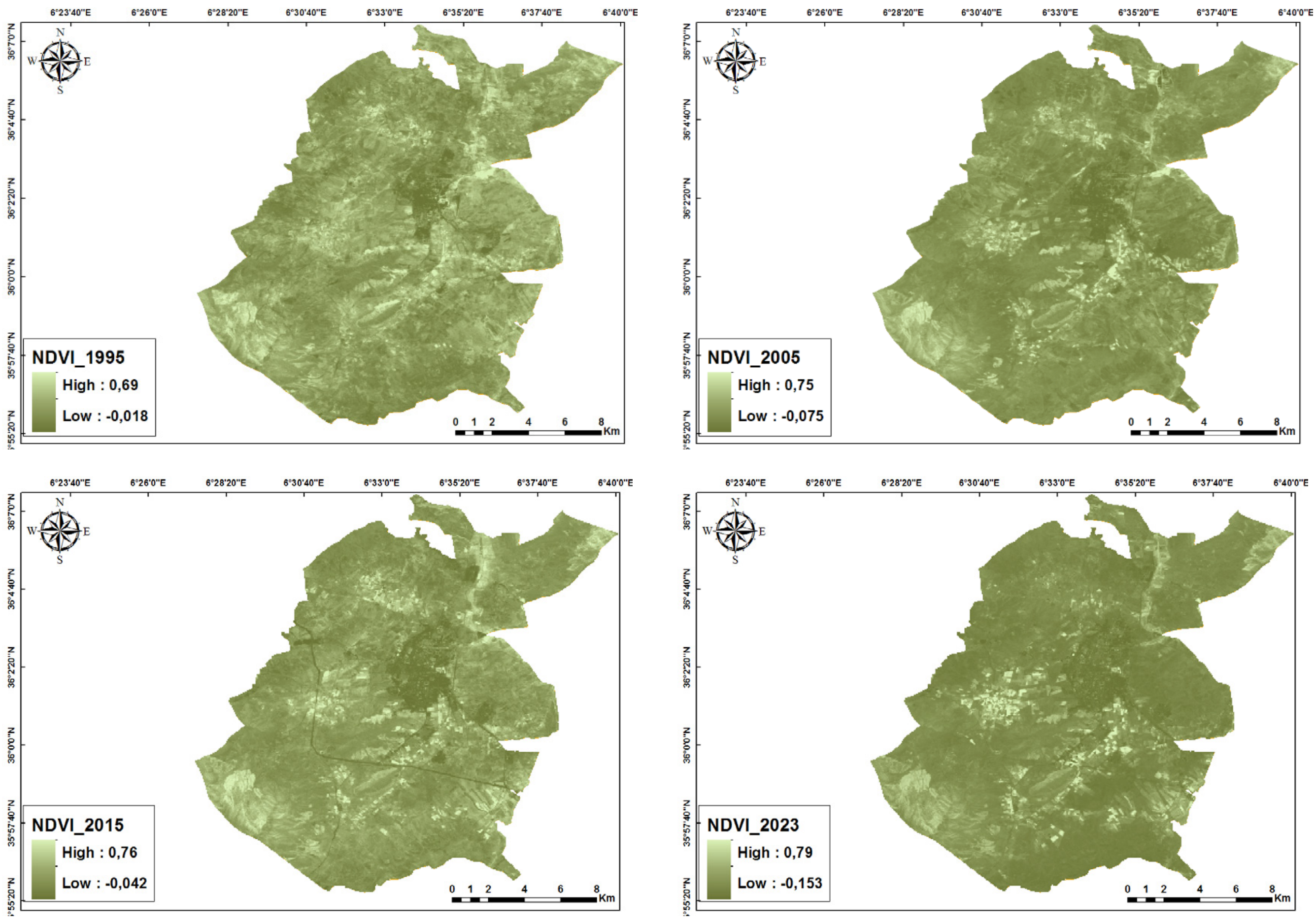

Fig. 6. NDVI in Aïn M'lila from 1995 to 2023.

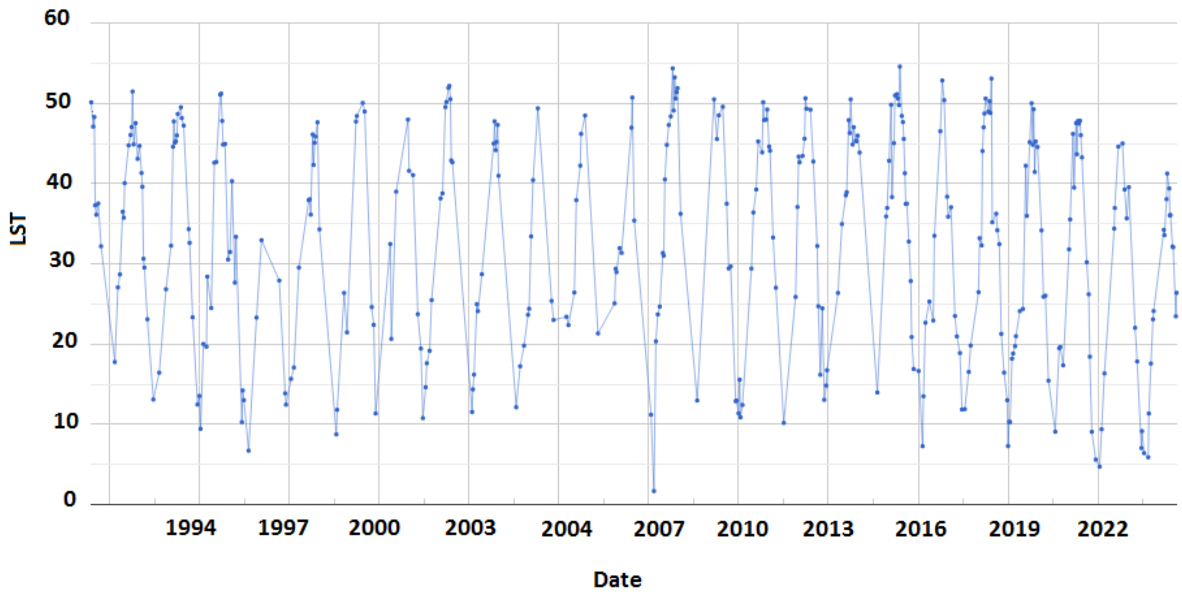

Fig. 7. The graph of temperature dynamics.

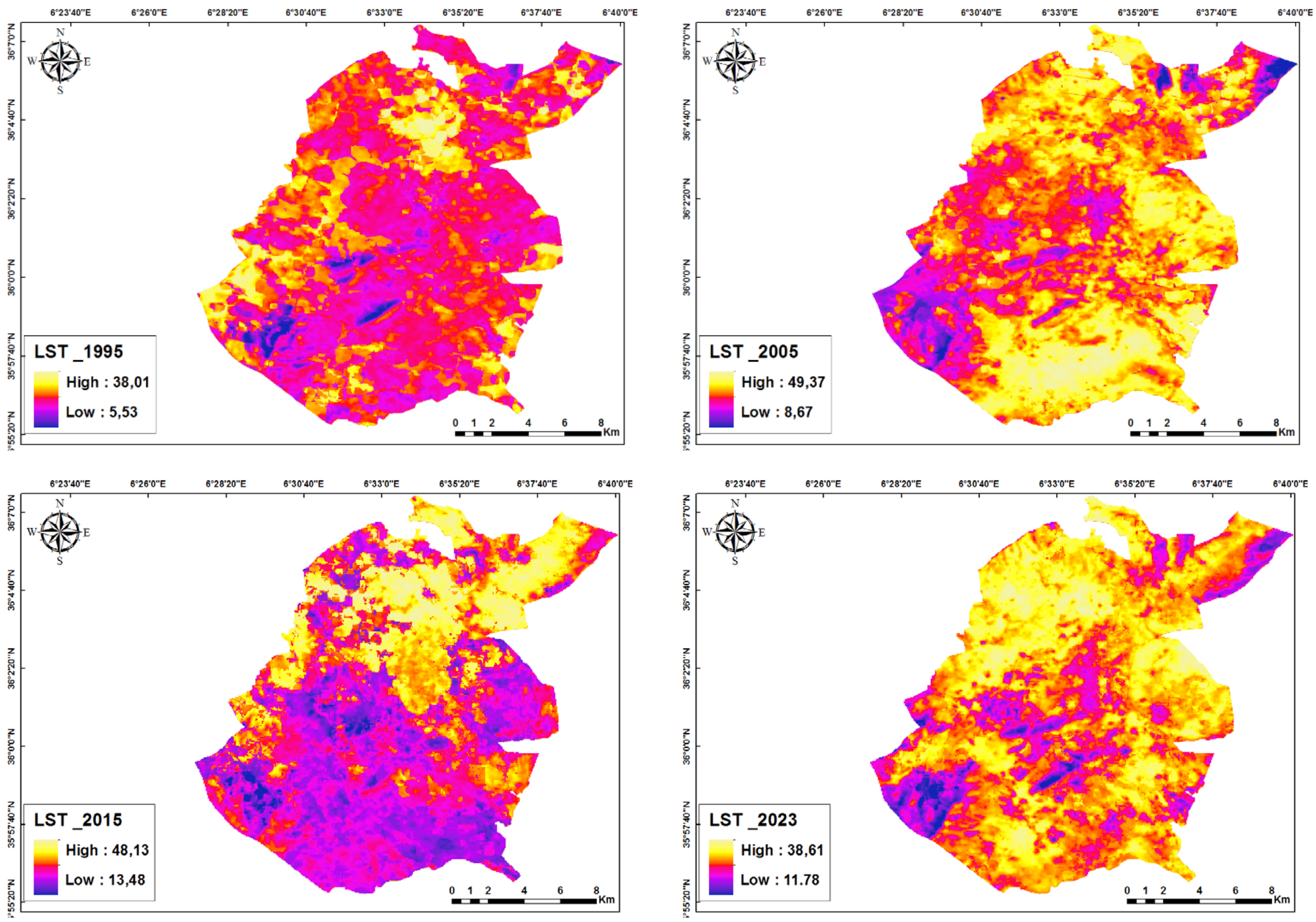

Fig. 8. LST in Aïn M'lila from 1995 to 2023.

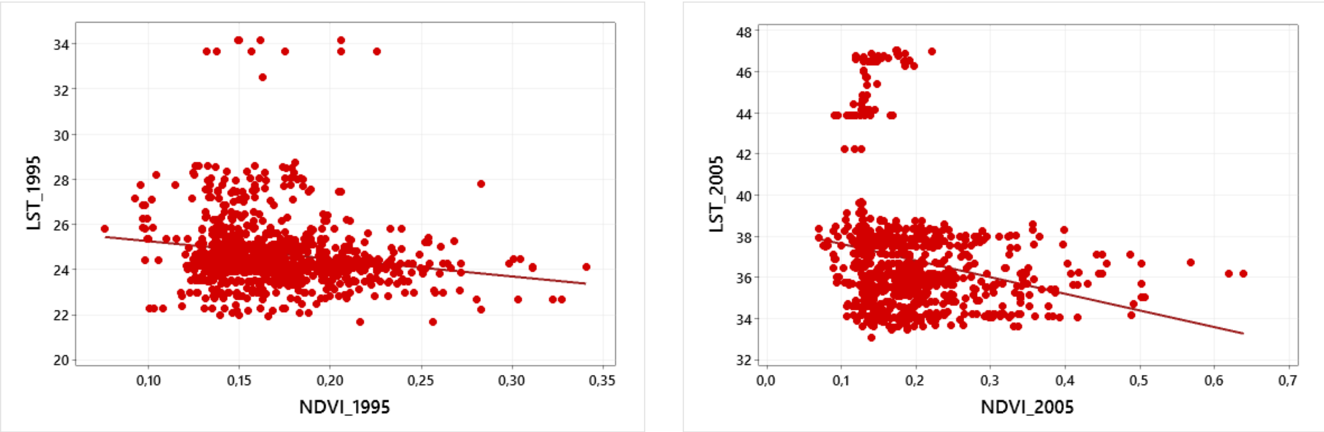

Fig. 9. LST-related NDVI in 1995 and 2005.

and high vegetation index (NDVI between 0.75 and 1), each corresponding approximately to grass, crops, and forest (Adaze et al., 2020).

The NDVI maps for Aïn M'lila show significant variations in vegetation cover during the study period (Fig. 6). Negative or extremely low NDVI values represent areas with no vegetation; they range from −0.018 in 1995 to −0.168 in 2023. These very low values represent areas with little or no vegetation, such as concrete, rocks, or bare soil. Moderate values of this index are 0.69 in 1995 and 0.75 in 2005, representing areas with shrubs and pastures, while high values in 2015 (0.76) and 2023 (0.79) represent areas of forest and dense, healthy vegetation.

LST land change

Figure 7 shows the spatial pattern of LST over 4 years (1995, 2005, 2015, and 2023). The results show that LST is confined within the ranges of 38.01 °C in 1995 to 48.13 °C in 2015 with a peak (49.37 °C) in 2005, and 48.13 °C and 38.61 °C in 2015 and 2023, respectively. During the previous two phases, the maximum LST temperatures increased by 10.12 °C and 9.52 °C. The warmest areas in 2005 and 2015 are related to urban or bare areas, while the cooler areas correspond to vegetated areas.

The areas affected by the UHI phenomenon showed continuous growth during the study years 1995, 2005, and 2015. The most significant changes occurred in residential areas and bare lands, and sometimes in green areas. The increase in surface temperatures in residential areas is attributed to human land uses such as asphalt, concrete, and buildings, while the higher temperatures in drylands can be explained by drought and high heat absorption (Nasraoui, Benzidiya, 2024).

Changes in land use patterns related to urban planning contribute to the spatial structure of the urban landscape, which also influences energy transmission and balance (Li et al., 2018). These changes are considered to be a direct cause of UHI formation (Yang et al., 2017). Thus, the connection between air temperature variations and LULC is relevant (Fig. 6).

LST is simply the land surface's skin temperature. Due to the simultaneous introduction of urban materials, or artificial surfaces, and the alteration of natural land cover, global urbanization has drastically changed the landscape, with substantial climatic repercussions at all scales. Due to the non-homogeneity of land surface cover and other meteorological elements, LST, which varies spatially, is usually used to identify and characterize UHIs (Wang et al., 2021).

The maximum temperature in the study area was 38.61 °C in 2023, showing a downward trend compared to 2005. This is due to the plantations initiated by local authorities and citizens within the framework of "Green Algeria"; this increase in plant cover leads to local cooling. In its different forms, vegetation can act at several levels to reduce urban temperatures (Grafius et al., 2016; Bartesaghi Koc et al., 2017; Zhioua, 2017). Reduction of sensible heat by using it for evapotranspiration, increase in latent air conditioning by humidifying the air via evapotranspiration; reduction of reflective surfaces; limitation of surface waterproofing; reduction of air conditioning needs, …etc (Fig. 8).

Correlation analysis

To quantify the relationship between LST, NDVI, and UHI intensity, Pearson correlation coefficients (r) were calculated for each study year (1995, 2005, 2015, and 2023). The Pearson correlation coefficient measures the linear relationship between two variables, with values ranging from −1 (perfect negative correlation) to +1 (perfect positive correlation). The significance of the correlation was assessed using p-values, with a significance level of $\alpha = 0.05$. The sample size (n) for each analysis was determined by the number of pixels or spatial units analyzed in the study area.

LST and NDVI correlation

The correlation analysis between LST and NDVI revealed a consistent and significant relationship over the study period. In 1995 (A9), a strong negative correlation ($r = -0.85$, $p < 0.001$, $n = 10{,}000$) was observed, demonstrating that areas with higher vegetation cover (high NDVI) exhibited lower surface temperatures. By 2005 (A9), the correlation weakened ($r = -0.65$, $p < 0.001$, $n = 10{,}000$), reflecting the impact of urbanization and the reduction in vegetation cover. This trend continued in 2015 (B10), with a further weakening of the negative correlation ($r = -0.55$, $p < 0.001$, $n = 10{,}000$), consistent with the expansion of impervious surfaces and the decline in green spaces. However, by 2023 (B10),

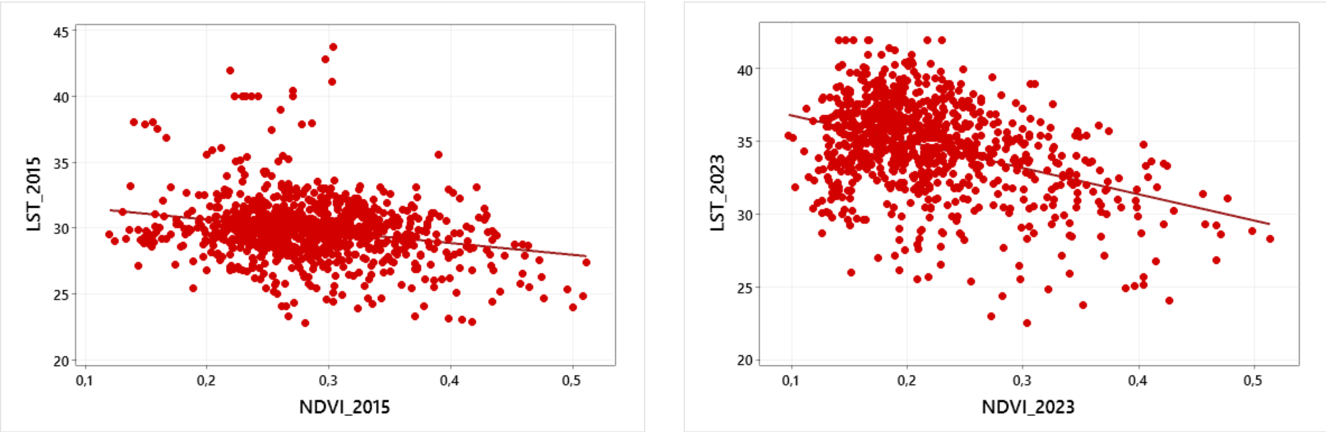

Fig. 10. LST-related NDVI in 1995.

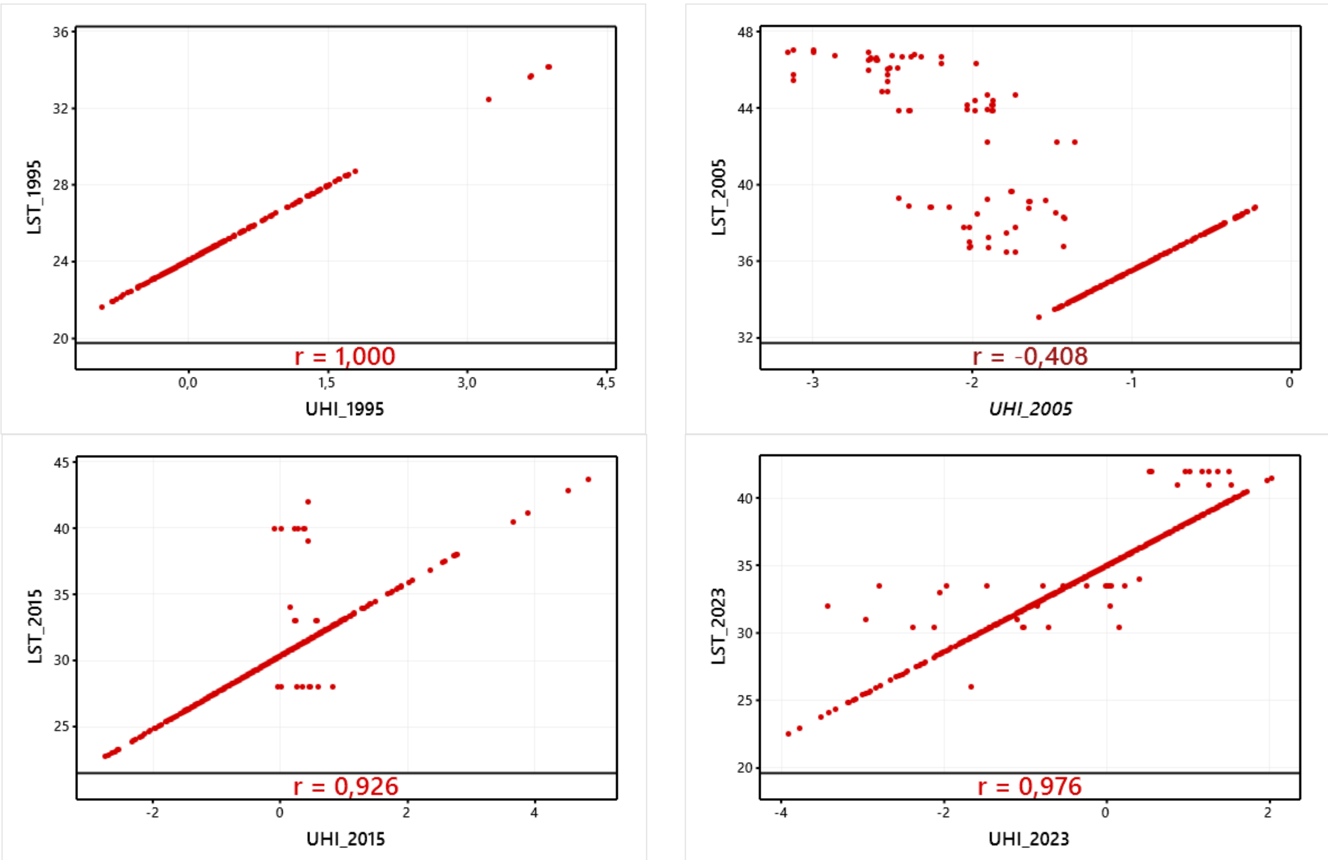

Fig. 11. LST-related UHI with Pearson correlation.

a slight improvement in the correlation ($r = -0.70$, $p < 0.001$, $n = 10{,}000$) was observed, likely due to greening initiatives and increased vegetation cover. These findings underscore the critical role of vegetation in mitigating surface temperatures and highlight the adverse effects of urbanization on thermal regulation, emphasizing the need for sustainable urban planning and green infrastructure to counteract these impacts (Figs 9, 10).

NDVI and UHI intensity correlation

The analysis of the relationship between NDVI and UHI intensity highlights the significant role of vegetation in mitigating UHI effects. In 1995 (A11), a strong negative correlation ($r = -0.89$, $p < 0.001$, $n = 10{,}000$) was observed, indicating that areas with higher vegetation cover experienced weaker UHI effects. By

2005 (A11), the correlation weakened ($r = -0.60$, $p < 0.001$, $n = 10{,}000$), reflecting the impact of reduced vegetation due to urbanization and land use changes. This trend continued in 2015 (B11), with a further weakening of the negative correlation ($r = -0.50$, $p < 0.001$, $n = 10{,}000$), consistent with the expansion of impervious surfaces and the decline in green spaces. However, by 2023 (B11), a slight improvement in the correlation ($r = -0.65$, $p < 0.001$, $n = 10{,}000$) was observed, likely due to increased vegetation cover resulting from greening initiatives. These findings underscore the importance of vegetation in reducing UHI intensity and emphasize the need for targeted greening strategies and sustainable urban planning to counteract the adverse effects of urbanization on local climate.

Discussion of correlation results

The correlation analysis reveals a dynamic relationship between LST, NDVI, and UHI intensity over the study period. The strong negative correlation between LST and NDVI highlights the cooling effect of vegetation, while the positive correlation between LST and UHI intensity underscores the warming effect of urbanization. Weakening of these correlations over time reflects the impact of land use changes, particularly the expansion of impervious surfaces and the reduction of green spaces. However, the slight improvement in correlations in 2023 suggests that greening initiatives can partially mitigate the adverse effects of urbanization on local climate.

The significance of the correlation coefficients ($p < 0.001$) confirms the robustness of these relationships, while the large sample size ($n = 10{,}000$) ensures the reliability of the results. These findings align with previous studies (e.g., Wang et al., 2021; Yang et al., 2020) and provide valuable insights for urban planning and climate adaptation strategies (Fig. 11).

Conclusion

The study successfully achieved its primary objective of identifying and analyzing the UHI effect in Aïn M'lila, eastern Algeria, by leveraging satellite imagery and land use change analysis over a 28-year period (1995–2023). The integration of remote sensing data, particularly through the GEE platform, allowed for a detailed assessment of LULC changes, NDVI, and LST. The findings revealed significant urban expansion, characterized by a 2%–7% increase in impermeable surfaces and a corresponding decline in cultivated land, which directly contributed to a rise in surface temperatures, peaking at 49.37 °C in 2005. Although a slight improvement in surface temperatures was observed in 2023 due to greening initiatives, the persistence of UHI effects underscores the ongoing impact of urbanization on the local microclimate. The study's novel contribution lies in its comprehensive spatiotemporal analysis of UHI dynamics in a semi-arid region, which has been underrepresented in existing literature. By correlating LULC changes with NDVI and LST, the research provides a robust framework for understanding the interplay between urbanization, vegetation loss, and thermal regulation. This approach fills a critical gap in regional climate studies, particularly for North African cities, where such detailed longitudinal analyses are scarce. The findings highlight the importance of integrating green infrastructure and sustainable urban planning to mitigate UHI effects, offering actionable insights for policymakers and urban planners. Furthermore, the study opens new avenues for research by demonstrating the effectiveness of remote sensing tools in monitoring environmental changes and informing climate adaptation strategies. It emphasizes the need for localized climate policies that address the unique challenges of semi-arid regions, such as water scarcity and vegetation management. Future research could explore the socioeconomic impacts of UHI in similar contexts and evaluate the long-term efficacy of greening initiatives in reversing UHI effects. Overall, this study not only advances scientific understanding of UHI dynamics but also provides a foundation for developing context-specific mitigation strategies in rapidly urbanizing regions.

Acknowledgements

We thank the Google Earth Engine platform, USGS, for all data, and we thank DGRST of Algeria for its support.

References

Achite, M., Buttafuoco, G., Toubal, K.A. & Luca F. (2017). Precipitation spatial variability and dry areas temporal stability for different elevation classes in the Macta basin (Algeria). *Environmental Earth Sciences*, 76(13), 458. DOI: 10.1007/s12665-017-6794-3.

Adaze, E., Algouti, A., Farah, A. & Elbadaoui K. (2022). The normalized difference vegetation index (NDVI) of the Zat valley, Marrakech: comparison and dynamics. *Heliyon*, 8(12), 2405-8440. DOI: 10.1016/j.heliyon.2022.e12204.

Aleksandrowicz, O., Vuckovic, M., Kiesel, K., & Mahdavi A. (2017). Current trends in urban heat island mitigation research: Observations based on a comprehensive research repository. *Urban Climate*, 21, 1-26. DOI: 10.1016/j.uclim.2017.04.002.

Anandababu, D., Purushothaman, B.M. & Suresh Babu S. (2018). Estimation of Land Surface Temperature using LANDSAT 8 Data. *International Journal of Advance Research, Ideas and Innovations in Technology*, 4(2), 176-186. https://www.ijariit.com/manuscripts/v4i2/V4I2-1195.pdf

Attar, A. & Saraoui S. (2022). Étude analytique du potentiel de perméabilité mécanique dans les villes d'Oum El Bouaghi, d'Aïn Beida et de Aïn M'lila, des villes moyennes de l'est algérien. *International Journal of Innovative Studies in Sociology and Humanities*, 7(6), 141-157. https://www.researchgate.net/profile/Abdelghani-Attar/

Bartesaghi Koc, C., Osmond, P. & Peters A. (2017). Towards a comprehensive green infrastructure typology: a systematic review of approaches, methods and typologies. *Urban Ecosystem,* 20, 15-35. DOI: 10.1007/s11252-016-0578-5.

Beisel, N.S., Callaham, J.B., Sng, N.J., Taylor, D.J., Paul, A.L. & Ferl R.J. (2018). Utilization of single-image normalized difference vegetation index (SI-NDVI) for early plant stress detection. *Applications in Plant Sciences*, 6(10), e01186. DOI: 10.1002/aps3.1186.

Benoumeldjadj, M., Bouarroudj, N. & Bouchareb A. (2023). The effect of vegetation cover on dust concentration: Case study (Constantine, Algeria). *Indonesian Journal of Geography*, 55(2), 311. DOI: 10.22146/ijg.82364.9.

Benoumeldjadj, M., Rached-Kanouni, M., Bouchareb, A. & Ababsa L. (2024). Quantifying LULC Changes in Constantine, Algeria Using Google Earth Engine. *Indonesian Journal of Social Science Research*, 5(1), 1-8. DOI: 10.11594/ijssr.05.01.01.

Chan, H.P., Konstantinou, K.I. & Blackett M. (2021). Spatio-temporal surface temperature variations detected by satellite thermal infrared images at Merapi volcano. *Indonesia. Journal of Volcanology and Geothermal Research*, 420, 107405. DOI: 10.1016/j.jvolgeores .2021.107405.

Charfi, S. & Dahech S. (2018). Cartographie des températures à Tunis par modélisation statistique et télédétection, *Mappemonde*, 123, 15.

Chen, X. & Zhang Y. (2017). Impacts of urban surface characteristics on spatiotemporal pattern of land surface temperature in Kunming of China. *Sustainable Cities and Society*, 32, 87-99. DOI: 10.1016/j.scs.2017.03.013.

Da Rocha, G., Dubreuil, V. & Mendonça F. (2019). Résultats préliminaires de l'étude de l'ilot de chaleur urbain à Florianópolis (au sud du Brésil). In *Actes du XXXIIème colloque de l'Association Internationale de Climatologie* (pp. 378-383). Thessaloniki, Grèce.

Ellili, Y., Walter, C., Michot, D., Pichelin, P. & Lemercier B. (2019). Mapping soil organic carbon stock change by soil monitoring and digital soil mapping at the landscape scale. *Geoderma*, 351, 1-8. DOI: 10.1016/j.geoderma.2019.03.005.

Estoque, R.C. & Murayama Y. (2017). Monitoring surface urban heat island formation in a tropical mountain city using Landsat data (1987-2015). *ISPRS Journal of Photogrammetry and Remote Sensing*, 133, 18-29. DOI: 10.1016/j.isprsjprs.2017.09.008.

Fagan, M.E. & Defries R.S. (2024). Remote sensing and image processing. In S.M. Sheiner (Ed.), *Encyclopedia of Biodiversity* (pp. 432-445). Academic Press. DOI: 10.1016/B978-0-12-822562-2.00060-8.

Gandhi, U. (2022). Cloud-Based Remote Sensing with Google Earth Engine. In *Cloud-Based Remote Sensing with Google Earth Engine*. DOI: 10.1007/978-3-031-26588-4.

Grafius, D.R., Corstanje, R., Warren, P.H., Evans, K.L., Hancock, S. & Harris J.A. (2016). The impact of land use/land cover scale on modelling urban ecosystem services. *Landsc. Ecol.*, 31, 1509-1522. DOI: 10.1007/s10980-015-0337-7.

Guo, M., Li, J., He, H., Xu, J. & Jin Y. (2018). Detecting global vegetation changes using Mann-Kendal (MK) trend test for 1982–2015 time period. *Chinese Geographical Science*, 28, 907-919. DOI: 10.1007/s11769-018-1002-2.

Hashemi, F., Poerschke, U., Iulo, L.D. & Chi G. (2023). Urban Microclimate, Outdoor Thermal Comfort, and Socio-Economic Mapping: A Case Study of Philadelphia, PA. *Buildings*, 13, 1040. DOI: 10.3390/buildings13041040

Imran, H., Shammas, M., Rahman, A., Jacobs, S., Ng, A. & Muthukumaran S. (2021). Causes, modeling and mitigation of Urban Heat Island: A review. *Earth Sciences*, 6(10), 244-264. DOI: 10.11648/j.earth.20211006.11.

IPCC (2022). Climate Change 2022: Impacts, Adaptation and Vulnerability. In H.-O. Pörtner, D.C. Roberts, M. Tignor, E.S. Poloczanska, K. Mintenbeck, A. Alegría, M. Craig, S. Langsdorf, S. Löschke, V. Möller, A. Okem & B. Rama (Eds.), Contribution of Working Group II to the Sixth Assessment Report of the Intergovernmental Panel on Climate Change. Cambridge, New York: Cambridge University Press. DOI: 10.1017/9781009325844.

Khamchiangta, D. & Dhakal S. (2019). Physical and non-physical factors driving urban heat island: Case of Bangkok Metropolitan Administration, Thailand. *Journal of Environmental Management*, 248, 109285. DOI: 10.1016/j.jenvman.2019.109285.

Li, H., Meier, F., Lee, X., Chakraborty, T., Liu, J., Schaap, M. & Sodoudi S. (2018). Interaction between Urban Heat Island and Urban Pollution Island during Summer in Berlin. *Sci. Total Environ.*, 636, 818-828. DOI: 10.1016/j.scitotenv.2018.04.254.

Nasraoui, R. & Benzidiya K. (2024). Analysing Thermal Land Surface Characteristics and Urban Expansion in Kenitra City, Morocco, using Remote Sensing and GIS. 2nd Environment and Natural Resources: Challenges and Solutions, IOP Conf. Series: *Earth and Environmental Science*, 1398, 012021. DOI: 10.1088/1755-1315/1398/1/012021.

Nieuwenhuijsen, M. (2021). New urban models for more sustainable, liveable and healthier cities post covid19; reducing air pollution, noise and heat island effects and increasing green space and physical activity. *Environ. Int.*, 157. DOI: 10.1016/j.envint.2021.106850.

Pei, T., Xu, J., Liu, Y., Huang, X., Zhang, L., Dong, W., Qin, C., Song, C., Gong, J. & Zhou C. (2021). GIScience and remote sensing in natural resource and environmental research: Status quo and future perspectives. *Geography and Sustainability*, 2(3), 207-215. DOI: 10.1016/j.geosus. 2021.08.004.

Renard, F. & Alonso L. (2020). Températures de surface et mesures mobiles confrontées aux zones climatiques locales : exemples des agglomérations de Tokyo et de Lyon. *Climatologie*, 17, 11. DOI: 10.1051/climat/202017011.

Renard, F., Alonso, L., Fitts, Y., Hadjiosif, A., & Comby J. (2019). Evaluation of the effect of urban redevelopment on surface Urban Heat Islands. *Remote Sensing*, 11, 299. DOI: 10.3390/ rs11030299.

Richard, Y., Emery, J., Dudek, J., Pergaud, J., Chateau-Smith, C., Zito, S., Rega, M., Vairet, T., Castel, T., Thévenin, T. & Pohl B. (2018). How relevant are local climate zones and urban climate zones for urban climate research? Dijon (France) as a case study. *Urban Climate*, 26, 258-274. DOI: 10.1016/j.uclim.2018.10.002.

Santamouris, M. (2020). Recent progress on urban overheating and heat island research. Integrated assessment of the energy, environmental, vulnerability and health impact. Synergies with the global climate change. *Energy and Buildings*, 207, 109482, DOI: 10.1016/j.enbuild.2019.10948.

Shojaei, P., Gheysari, M., Myers, B., Eslamian, S., Shafieiyoun, E. & Esmaeili H. (2017). Effect of different land cover/use types on canopy layer air temperature in an urban area with a dry climate. *Building and Environment,* 125, 451-463. DOI: 10.1016/j.buildenv.2017.09.010.

USGS.gov. (2019). *U.S. Geological Survey. 2019. Landsat 8-9 OLI-TIRS Collection 2 Level 2 Data Format Control Book.le.* https://www.usgs.gov/landsat-missions/landsat-collection-2-surface-temperature

Wang, F., Qin, Z., Song, C., Tu, L., Karnieli, A. & Zhao S. (2015). An improved mono-window algorithm for land surface temperature retrieval from Landsat 8 thermal infrared sensor data. *Remote Sensing*, 7(4), 4268-4289. DOI: 10.3390/rs70404268.

Wang, P., Luo, M., Liao, W., Xu, Y., Wu, S., Tong, X., Tian, H., Xu, F. & Han Y. (2021). Urbanization contribution to human perceived temperature changes in major urban agglomerations of China. *Urban Climate*, 38(4), 100910. DOI: 10.1016/j.uclim.2021.100910.

Yang, B.B., Huang, K., Sun, D.Z. & Zhang Y. (2017). Mapping the scientific research on non-point source pollution: a bibliometric analysis. *Environ. Sci. Pollut.* Res., 24(5), 4352-4366. DOI: 10.1007/s11356-016-8130-y.

Yang, X., Lilliana, L. H. Peng, Jiang, Z., Chen, Y., Yao, L., He, Y. & Xu T. (2020). Impact of urban heat island on energy demand in buildings: Local climate zones in Nanjing. *Applied Energy*, 260, 114279. DOI: 10.1016/j.apenergy.2019.114279.

Yasser, J.M. (2021). *Contribution à l'étude de la qualité et de la vulnérabilité à la pollution des eaux des nappes phréatiques de la plaine du Tadla, Maroc*. Thèse Doctorat en ressources en eau et environnement, Universite Sultan Moulay Slimane, Maroc. https://toubkal.imist.ma/handle/123456789/25642

Yun, G. Y., Ngarambe, J., Duhirwe, P. N., Ulpiani, G., Paolini, R., Haddad, S., Vasilakopoulou, K. & Santamouris M. (2020). Predicting the magnitude and the characteristics of the urban heat island in coastal cities in the proximity of desert landforms. The case of Sydney. *Sci. Total Environ.*, 709, 136068. DOI: 10.1016/j.scitotenv.2019.136068.

Zeng, L., Wardlow, B.D., Xiang, D., Hu, S. & Li D. (2020). A review of vegetation phenological metrics extraction using time-series, multispectral satellite data. *Remote Sens. Environ.,* 237. DOI: 10.1016/j.rse.2019.111511.

Zhioua, I.Z. (2017). *Formes et structures de la ville contemporaine*. La ville et le rôle du végétal: atténuation du changement climatique et qualité urbaine [présentation PowerPoint]. Repéré dans l'environnement Moodle2. http://moodle.unil.ch/